JACS
JOURNAL OF THE AMERICAN CHEMICAL SOCIETY
pubs.acs.org/JACS
Communication

Operando Resonant Soft X-ray Scattering Studies of Chemical Environment and Interparticle Dynamics of Cu Nanocatalysts for CO_2 Electroreduction

Yao Yang, Inwhan Roh, Sheena Louisia, Chubai Chen, Jianbo Jin, Sunmoon Yu, Miquel B. Salmeron, Cheng Wang,* and Peidong Yang*

Cite This: *J. Am. Chem. Soc.* 2022, 144, 8927−8931
Read Online
ACCESS | Metrics & More | Article Recommendations | Supporting Information

ABSTRACT: Understanding the chemical environment and interparticle dynamics of nanoparticle electrocatalysts under operating conditions offers valuable insights into tuning their activity and selectivity. This is particularly important to the design of Cu nanocatalysts for CO_2 electroreduction due to their dynamic nature under bias. Here, we have developed *operando* electrochemical resonant soft X-ray scattering (EC-RSoXS) to probe the chemical identity of active sites during the dynamic structural transformation of Cu nanoparticle (NP) ensembles through 1 μm thick electrolyte. *Operando* scattering-enhanced X-ray absorption spectroscopy (XAS) serves as a powerful technique to investigate the size-dependent catalyst stability under beam exposure while monitoring the potential-dependent surface structural changes. Small NPs (7 nm) in aqueous electrolyte were found to experience a predominant soft X-ray beam-induced oxidation to CuO despite only sub-second X-ray exposure. In comparison, large NPs (18 nm) showed improved resistivity to beam damage, which allowed the reliable observation of surface Cu_2O electroreduction to metallic Cu. Small-angle X-ray scattering (SAXS) statistically probes the particle−particle interactions of large ensembles of NPs. This study points out the need for rigorous examination of beam effects for *operando* X-ray studies on electrocatalysts. The strategy of using EC-RSoXS that combines soft XAS and SAXS can serve as a general approach to simultaneously investigate the chemical environment and interparticle information on nanocatalysts.

The CO_2 reduction reaction (CO_2RR) has emerged as a promising renewable technology to convert greenhouse gas into liquid fuels and chemicals.[1,2] Among many heterogeneous electrocatalysts investigated, Cu is the predominant candidate for selective CO_2 electroreduction to multicarbon products (C_{2+}).[3−5] However, understanding of the nature of active sites under reaction conditions has remained limited, particularly for high-performance Cu nanocatalysts,[6,7] which calls for further development of *operando*/*in situ* methods.[8] Hard X-ray absorption spectroscopy (XAS) has been widely used to investigate the structural changes of bulk electrocatalysts,[9−16] due to the high penetration of high-energy X-rays and relatively low beam damage.[17,18] However, hard XAS (>5 keV) can only probe core electrons of the Cu atoms, which are not actively participating during electrocatalysis.[8,17] In comparison, soft XAS (<1 keV) can probe valence electrons (e.g., 3d electrons) by using transition metal L-edges, which are chemically more relevant in electrocatalysis.[19,20] Soft XAS is typically collected in either surface-sensitive total electron yield (TEY) mode or total fluorescence yield (TFY) mode that collects bulk signals.[21−23] Given the ultrahigh vacuum required for soft X-ray, it remains a great challenge to design a liquid cell that can enable reliable electrochemistry and simultaneous acquisition of sufficiently strong X-ray signals.[23−27] The few *in situ* soft XAS studies have investigated bulk Cu electrodes in TFY modes and delivered limited structural insights due to the weak X-ray signals[28] or undesirable beam-induced damage caused by the large absorption cross section of soft X-rays.[29]

Inspired by resonant soft X-ray scattering studies for polymer−polymer interactions,[30−32] here, we have designed an *operando* electrochemical RSoXS (EC-RSoXS) that combines *in situ* soft XAS and small-angle X-ray scattering (SAXS). *In situ* soft XAS enables a high sensitivity of the chemical valence of a material with sub-second X-ray pulses. Meanwhile, SAXS serves as a unique tool to statistically probe the particle−particle interactions of Cu NP ensembles.

To elucidate the dynamic surface structures of Cu nanocatalysts under electroreduction, we employed *operando* EC-RSoXS to track the chemical environment, specifically, the chemical valence of Cu, in this study. Figure 1a presents a cross-section of the *operando* X-ray cell, which allows the simultaneous acquisition of XAS and SAXS spectra under real-time electrochemical conditions. The two assembled microchips encapsulate a liquid layer of 1 μm, which is sufficiently thin to enable soft X-ray study in a transmission mode (Figure S1a,b). The X-ray cell is composed of three electrodes, including a glassy carbon working electrode (WE) for depositing nanocatalysts and Pt counter and pseudo-reference

Received: April 5, 2022
Published: May 16, 2022

https://doi.org/10.1021/jacs.2c03662
J. Am. Chem. Soc. 2022, 144, 8927−8931

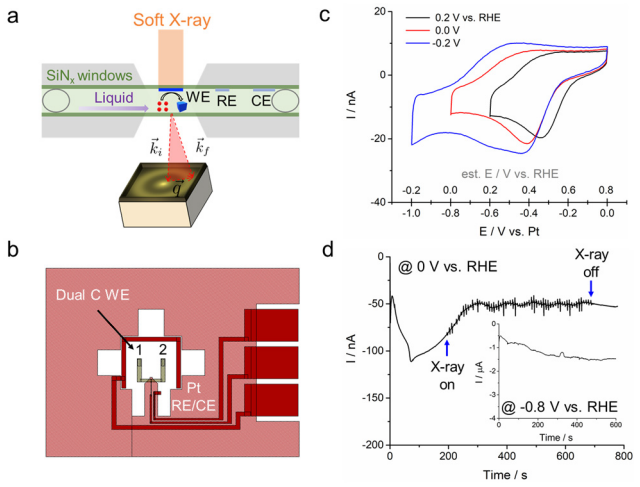

Figure 1. *Operando* electrochemical liquid-cell resonant soft X-ray scattering (EC-RSoXS) setup. (a) Schematic of the X-ray cell with the capability to enable reliable electrochemistry and simultaneously acquire soft XAS and SAXS through 1 μm liquid. (b) Design of the X-ray microchip with dual carbon WE, and Pt RE and CE. (c) CV profiles of Cu NPs at 100 mV/s in CO_2-saturated 0.1 M $KHCO_3$ with different lower potential limits. (d) CA profiles of Cu NPs at 0 and −0.8 V (inset) vs RHE.

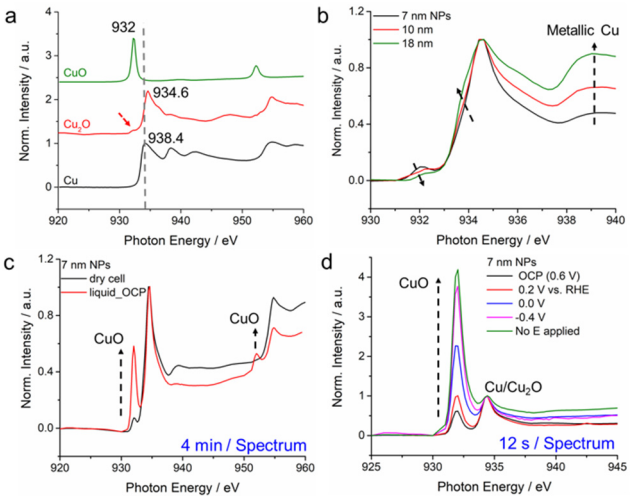

Figure 2. *Operando* soft XAS of the 7 nm NP ensemble in electrolyte under X-ray exposure. (a) XAS spectra of standard references and (b) 7, 10, and 18 nm NP ensembles. (c) XAS spectra of the 7 nm NP ensemble showing beam-induced oxidation to CuO in liquid. (d) *Operando* XAS spectra of the 7 nm NP ensemble under applied potentials from 0.2 to −0.4 V vs RHE, showing that X-ray-induced oxidation overwhelmed electroreduction.

electrodes (CE and RE) (Figure 1b). The potential of the Pt pseudo-RE was estimated to be ∼0.8 V vs the reversible hydrogen electrode (RHE).[33−35] The customized design of the X-ray microchip used in this study includes dual glassy carbon windows that allow us to rigorously assess the soft X-ray beam effects (Figures 1c and S1c). The NPs deposited on the left glassy carbon (GC) window 1 are exposed to the X-ray beam, while the NPs deposited on the right window 2 serve as a control group, which experiences the same electrochemical conditions but without X-ray exposure (Figure S1c). The cyclic voltammetric (CV) profiles of as-synthesized 7 nm Cu@Cu_2O NPs, with a metallic Cu core surrounded by a ∼2 nm Cu_2O shell, show well-defined reduction peaks of surface Cu_2O at ∼0.45 V vs RHE in the EC-RSoXS cell, which match well with standard H-cell measurements (Figures S2 and S3). The chronoamperometry (CA) profile of 7 nm NPs at 0 V shows a stable current plateau of ∼50 nA (Figure 1d). When soft X-ray was turned on as the current stabilized after 200 s, periodic minor current spikes (<10 nA) emerged, likely due to photoelectrons generated by X-ray pulses.[29] Such a minor interference did not alter the average current plateau and disappeared once the beam was turned off. More importantly, the photoelectron-induced current is negligible when compared to the stable μA-level current at −0.8 V, which simulates the typical operating condition for CO_2 electroreduction to C_{2+} products. Similar current plateaus were also observed for the 18 nm Cu NP ensemble (Figure S4).

Given the reliability of our electrochemical measurements, we then carried out soft XAS measurements. The Cu $L_{3,2}$ edges in the XAS of Cu foil, Cu_2O and CuO powders were first measured (Figure 2a). The L_3 edges (∼934 eV) and L_2 edges (∼952 eV) correspond to Cu $2p^{3/2}\rightarrow 3d^{3/2}3d^{5/2}$ and $2p^{1/2}\rightarrow 3d^{3/2}$ transitions, respectively. Metallic Cu foil shows the characteristic triplet peaks at 934.4 eV (2p→3d transition) and 938.4, 942.2 eV (2p→4s,p transition) due to the hybridization of Cu d and s,p orbitals (Figure S5). Cu_2O shows a major peak at 934.6 eV and a minor peak at 932.0 eV (indicated by the red arrow), which are consistent with previous studies.[26] CuO exhibits strong peaks at 932.2 and 952.3 eV. The XAS spectrum of clean Cu foil was collected in TEY mode, and the other two references were collected in TFY mode (Figure S6). Soft XAS of as-synthesized NPs in TFY mode show an increasing metallic Cu fraction as particle size increases from 7 to 18 nm, as indicated by the arrow at 938.4 eV and a slight negative shift of the main edge from 934.6 to 934.4 eV, as well as a decay of the oxide feature at 932.0 eV (Figure 2b). The increasing metallic fraction of larger NPs was also supported by powder X-ray diffraction (Figure S7), and the surface Cu_2O layer was measured to be ∼2 nm for 18 nm NPs based on atomic-scale electron energy loss spectroscopy elemental mapping (Figure S8).

Operando soft XAS was performed to investigate the chemical valence of 7 nm Cu@Cu_2O NPs under electroreduction. The well-resolved XAS spectrum in liquid demonstrates the advantage of scattering-enhanced XAS (Figure 2c), where the total scattered signal was collected with an area detector in comparison to conventional transmission XAS (Figure S9). However, when the electrolyte was introduced in the cell, the 7 nm Cu NPs ensemble showed the beam-induced oxidation from Cu@Cu_2O to CuO after only 4 min of acquisition (Figures 2c and S10). This surprising observation is consistent with recent studies by Salmeron et al., where the soft X-ray beam was reported to completely oxidize a bulk Cu film to CuO in alkaline media (Figure S11).[29] This observation was suggested to result from the formation of oxidative radicals (e.g., •OH) generated by soft X-ray-induced photoelectrons in water.[29] The smaller Cu NPs studied here are thus much more susceptible than bulk Cu to beam-induced oxidation to CuO in water. Subsequent XAS spectra at potentials from 0 to −0.4 V only showed the continuous increase of the CuO peak due to accumulating beam-induced oxidation (Figure 2d). In comparison, *operando* soft XAS of the 18 nm Cu NPs ensemble showed much less beam damage within the first four spectra in addition to a minor formation of metallic Cu (Figure S12). These results suggest that 18 nm

https://doi.org/10.1021/jacs.2c03662
J. Am. Chem. Soc. 2022, 144, 8927−8931

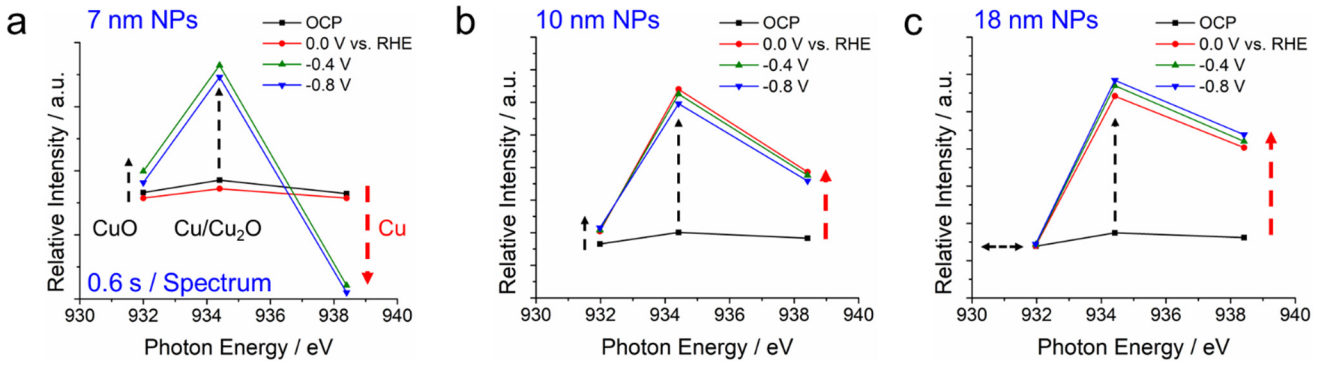

Figure 3. *Operando* XAS of Cu ensembles with sub-second X-ray pulses. (a) *Operando* XAS of the 7 nm Cu NPs ensemble in liquid, with three X-ray pulses still showing significant beam-induced oxidation to CuO. (b, c) *Operando* XAS of the 10 and 18 nm NP ensembles, showing minor and negligible beam-induced oxidation, respectively. The latter enables the observation of surface Cu_2O electroreduction to metallic Cu.

NPs are more resistive to beam-induced oxidation, relative to the 7 nm NPs, and the electrochemical reduction could largely counteract the X-ray beam damage. Further XAS acquisition on the 18 nm Cu NPs ensemble showed that X-ray-induced oxidation overwhelmed the XAS spectra once the applied potentials were turned off (Figure S13).

The ultrahigh sensitivity of scattering-enhanced XAS allowed the acquisition time to be further lowered to 0.2 s. Cu NPs were only exposed to X-ray for a total of 0.6 s to acquire three key data points at characteristic energy values of CuO (932.0 eV), Cu/Cu_2O (934.4 eV), and Cu (938.4 eV) (Figure 3). Despite only sub-second X-ray exposure, 7 nm NPs still showed significant beam-induced oxidation to CuO, as evidenced by the intensity increase of the CuO peak and the decrease of the Cu peak (Figure 3a). In comparison, the 10 nm Cu NPs ensemble began to exhibit the electroreduction of Cu_2O to Cu but with a minor increase of the CuO peak, suggesting partially suppressed beam-induced oxidation (Figure 3b). Finally, the 18 nm Cu NPs ensemble consistently showed the electrochemical reduction from surface Cu_2O to Cu with negligible beam-induced oxidation (Figure 3c). Full XAS spectra of the 18 nm Cu NP ensemble in the first window after X-ray pulses exhibited nearly the same spectroscopic features as observed in the second window without X-ray pulses, suggesting that sub-second X-ray exposure caused negligible beam-induced damage on 18 nm Cu NPs (Figure S14).

Small-angle X-ray scattering (SAXS) was then employed to investigate the particle−particle interaction of the NPs ensembles. SAXS spectra of as-synthesized NPs show distinct scattering patterns (Figure 4a). Basic scattering analysis can be conducted based 2D hexagonal-packed spherical nanoparticles.

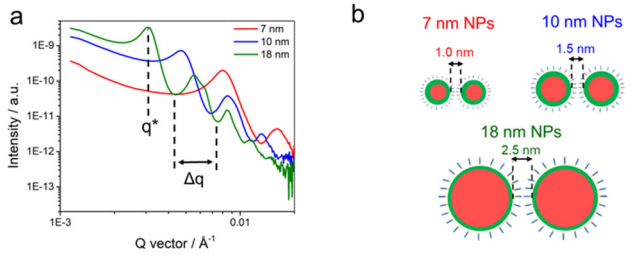

Figure 4. Soft SAXS studies of NP ensembles: (a) SAXS spectra of as-synthesized NPs. The differences between q^* and Δq were used to calculate the interparticle distances, as shown in the scheme in (b).

The q^* at the first maximum peak measures the average particle−particle distance, and the Δq of the distance between two minimum peaks measures the average particle diameter. Assuming a solid spherical particle coated with ligand, the difference between q^* and Δq is the interparticle distance (Table S1). As the particle size increases from 7 to 10 and 18 nm, the interparticle distance increases from 1.0 to 1.5 and 2.5 nm, respectively (Figure 4b). The smaller gap among the assembled 7 nm NPs, relative to that of 18 nm NPs, is consistent with the smaller interparticle distances observed in STEM images (Figure S7b,c). It implies a stronger tetradecylphosphonic acid (TDPA) ligand−ligand interaction within narrower gaps among smaller NPs and a higher degree of ligand interdigitation, which was also observed on ligand-coated Ag NPs in our recent vibrational spectroscopy study.[36] *Operando* SAXS shows the potential to probe dynamic evolution of particle−particle interactions under electrochemical conditions, which will be included in our future study.

In conclusion, this study presents a technical breakthrough of EC-RSoXS to combine *operando* soft XAS and SAXS to probe the valence state and particle−particle interactions of Cu NP ensembles under electrochemical conditions. To mitigate soft X-ray beam effects, several approaches have been proposed.[29] For instance, a flow cell can be designed to constantly supply fresh electrolyte to minimize the accumulation oxidative radicals,[27] ultrafast X-ray shutter, continuous scanning of the monochromator, and a defocused beam can help lower the dead time and reduce the effective X-ray dose per unit area.[37,38] In this work, the enhancement of spectroscopy and scattering signal with the statistical ensemble of NPs is the key to the minimization of the averaged dose, which in turn mitigates beam-induced artifacts. We anticipate that the continuous development of *operando* soft X-ray methods will play an instrumental role in elucidating the nature of active sites of electrocatalysts.

■ ASSOCIATED CONTENT

Supporting Information

The Supporting Information is available free of charge at https://pubs.acs.org/doi/10.1021/jacs.2c03662.

Materials and methods, Figures S1−S14, and Table S1 (PDF)

https://doi.org/10.1021/jacs.2c03662
J. Am. Chem. Soc. 2022, 144, 8927−8931

AUTHOR INFORMATION

Corresponding Authors

Peidong Yang − *Department of Chemistry, University of California, Berkeley, California 94720, United States; Chemical Sciences Division, Lawrence Berkeley National Laboratory, Berkeley, California 94720, United States; Department of Materials Science and Engineering, University of California, Berkeley, California 94720, United States; Materials Sciences Division, Lawrence Berkeley National Laboratory, Berkeley, California 94720, United States; Kavli Energy NanoScience Institute, Berkeley, California 94720, United States;* orcid.org/0000-0003-4799-1684; Email: p_yang@berkeley.edu

Cheng Wang − *Advanced Light Source, Lawrence Berkeley National Laboratory, Berkeley, California 94720, United States;* orcid.org/0000-0001-7192-5471; Email: cwang2@lbl.gov

Authors

Yao Yang − *Department of Chemistry, University of California, Berkeley, California 94720, United States; Miller Institute for Basic Research in Science, University of California, Berkeley, California 94720, United States; Chemical Sciences Division, Lawrence Berkeley National Laboratory, Berkeley, California 94720, United States;* orcid.org/0000-0003-0321-3792

Inwhan Roh − *Department of Chemistry, University of California, Berkeley, California 94720, United States;* orcid.org/0000-0001-7337-4458

Sheena Louisia − *Department of Chemistry, University of California, Berkeley, California 94720, United States; Chemical Sciences Division, Lawrence Berkeley National Laboratory, Berkeley, California 94720, United States;* orcid.org/0000-0002-2175-6769

Chubai Chen − *Department of Chemistry, University of California, Berkeley, California 94720, United States;* orcid.org/0000-0003-2513-2707

Jianbo Jin − *Department of Chemistry, University of California, Berkeley, California 94720, United States;* orcid.org/0000-0002-9054-7960

Sunmoon Yu − *Chemical Sciences Division, Lawrence Berkeley National Laboratory, Berkeley, California 94720, United States; Department of Materials Science and Engineering, University of California, Berkeley, California 94720, United States;* orcid.org/0000-0001-7250-9365

Miquel B. Salmeron − *Department of Materials Science and Engineering, University of California, Berkeley, California 94720, United States; Materials Sciences Division, Lawrence Berkeley National Laboratory, Berkeley, California 94720, United States;* orcid.org/0000-0002-2887-8128

Complete contact information is available at: https://pubs.acs.org/10.1021/jacs.2c03662

Notes

The authors declare no competing financial interest.

ACKNOWLEDGMENTS

This work was supported by Director, Office of Science, Office of Basic Energy Sciences, Chemical Sciences, Geosciences, & Biosciences Division, of the U.S. Department of Energy under Contract DE-AC02-05CH11231, FWP CH030201 (Catalysis Research Program). This research used resources described above of the Advanced Light Source, which is a DOE Office of Science User Facility under Contract No. DE-AC02-05CH11231. This work used TEM facilities at the Molecular Foundry, supported by the Office of Science, Office of Basic Energy Sciences, of the U.S. Department of Energy under Contract No. DE-AC02-05CH11231. Y.Y. acknowledges support from the Miller Research Fellowship (2021-2024). J.J. and C.C. acknowledge support from the Suzhou Industrial Park Scholarship. S.Y. acknowledges support from Samsung Scholarship. We thank Dr. Isvar Cordova at the ALS for the help in chip design. We appreciate Dr. John Damiano at Protochips, Inc. for the long-term technical support.

REFERENCES

(1) Ross, M. B.; De Luna, P.; Li, Y.; Dinh, C.-T.; Kim, D.; Yang, P.; Sargent, E. H. Designing materials for electrochemical carbon dioxide recycling. *Nat. Catal.* **2019**, *2*, 648−658.

(2) Birdja, Y. Y.; Pérez-Gallent, E.; Figueiredo, M. C.; Göttle, A. J.; Calle-Vallejo, F.; Koper, M. T. M. Advances and challenges in understanding the electrocatalytic conversion of carbon dioxide to fuels. *Nat. Energy* **2019**, *4*, 732−745.

(3) Li, C. W.; Ciston, J.; Kanan, M. W. Electroreduction of Carbon Monoxide to Liquid Fuel on Oxide-Derived Nanocrystalline Copper. *Nature* **2014**, *508*, 504−507.

(4) Wakerley, D.; Lamaison, S.; Wicks, J.; Clemens, A.; Feaster, J.; Corral, D.; Jaffer, S. A.; Sarkar, A.; Fontecave, M.; Duoss, E. B.; Baker, S.; Sargent, E. H.; Jaramillo, T. F.; Hahn, C. Gas Diffusion Electrodes, Reactor Designs and Key Metrics of Low-Temperature CO_2 Electrolysers. *Nat. Energy* **2022**, *7*, 130−143.

(5) Arán-Ais, R. M.; Scholten, F.; Kunze, S.; Rizo, R.; Roldan Cuenya, B. The Role of In Situ Generated Morphological Motifs and Cu(I) Species in C_{2+} Product Selectivity during CO_2 Pulsed Electroreduction. *Nat. Energy* **2020**, *5*, 317−325.

(6) Kim, D.; Kley, C. S.; Li, Y.; Yang, P. Copper Nanoparticle Ensembles for Selective Electroreduction of CO_2 to C_2−C_3 products. *Proc. Natl. Acad. Sci. U.S.A.* **2017**, *114*, 10560−10565.

(7) Li, Y.; Kim, D.; Louisia, S.; Xie, C.; Kong, Q.; Yu, S.; Lin, T.; Aloni, S.; Fakra, S.; Yang, P. Electrochemically scrambled nanocrystals are catalytically active for CO_2-tomulticarbons. *Proc. Natl. Acad. Sci. U.S.A.* **2020**, *117*, 9194−9201.

(8) Yang, Y.; Xiong, Y.; Zeng, R.; Lu, X.; Krumov, M.; Huang, X.; Xu, W.; Wang, H.; DiSalvo, F. J.; Brock, J. D.; Muller, D. A.; Abruña, H. D. *Operando* Methods in Electrocatalysis. *ACS Catal.* **2021**, *11*, 1136−1178.

(9) Vavra, J.; Shen, T. H.; Stoian, D.; Tileli, V.; Buonsanti, R. Real-time Monitoring Reveals Dissolution/Redeposition Mechanism in Copper Nanocatalysts during the Initial Stages of the CO_2 Reduction Reaction. *Angew. Chem., Int. Ed.* **2021**, *60*, 1347−1354.

(10) Li, J.; et al. Copper Adparticle Enabled Selective Electrosynthesis of n-Propanol. *Nat. Commun.* **2018**, *9*, 4614.

(11) Chang, C.-J.; Lin, S.-C.; Chen, H.-C.; Wang, J.; Zheng, K. J.; Zhu, Y.; Chen, H. M. Dynamic Reoxidation/Reduction-Driven Atomic Interdiffusion For Highly Selective CO_2 Reduction Toward Methane. *J. Am. Chem. Soc.* **2020**, *142*, 12119−12132.

(12) Yang, Y.; Wang, Y.; Xiong, Y.; Huang, X.; Shen, L.; Huang, R.; Wang, H.; Pastore, J. P.; Yu, S. H.; Xiao, L.; Brock, J. D.; Zhuang, L.; Abruña, H. D. In Situ X-Ray Absorption Spectroscopy of a Synergistic Co-Mn Oxide Catalyst for the Oxygen Reduction Reaction. *J. Am. Chem. Soc.* **2019**, *141*, 1463−1466.

(13) Xiong, Y.; Yang, Y.; Feng, X.; DiSalvo, F. J.; Abruña, H. D. A Strategy for Increasing the Efficiency of the Oxygen Reduction Reaction in Mn-Doped Cobalt Ferrites. *J. Am. Chem. Soc.* **2019**, *141*, 4412−4421.

(14) Kimura, K. W.; Casebolt, R.; DaSilva, J. C.; Kauffman, E.; Kim, J.; Dunbar, T. A.; Pollock, C. J.; Suntivich, J.; Hanrath, T. Selective Electrochemical CO_2 Reduction during Pulsed Potential Stems from Dynamic Interface. *ACS Catal.* **2020**, *10*, 8632−8639.

(15) Geng, S.-K.; Zheng, Y.; Li, S.-Q.; Su, H.; Zhao, X.; Hu, J.; Shu, H.-B.; Jaroniec, M.; Chen, P.; Liu, Q.-H.; Qiao, S.-Z. Nickel Ferrocyanide as a High-Performance Urea Oxidation Electrocatalyst. *J. Am. Chem. Soc.* **2021**, *6*, 904−912.
(16) Vasileff, A.; Zhu, Y.; Zhi, X.; Zhao, Y.; Ge, L.; Chen, H. M.; Zheng, Y.; Qiao, S.-Z. Electrochemical Reduction of CO_2 to Ethane through Stabilization of an Ethoxy Intermediate. *Angew. Chem., Int. Ed.* **2020**, *59*, 19649−19653.
(17) Abruña, H. D.; White, J. H.; Albarelli, M. J.; Bommarito, G. M.; Bedzyk, M. J.; McMillan, M. Is There Any Beam Yet? Uses of Synchrotron Radiation in the in Situ Study of Electrochemical Interfaces. *J. Phys. Chem.* **1988**, *92*, 7045−7052.
(18) Yang, Y.; et al. Electrocatalysis in Alkaline Media and Alkaline Membrane-Based Energy Technologies. *Chem. Rev.* **2022**, *122*, 6117.
(19) Smith, J. W.; Saykally, R. J. Soft X-ray Absorption Spectroscopy of Liquids and Solutions. *Chem. Rev.* **2017**, *117*, 13909−13934.
(20) Beaumont, S. K. Soft XAS as an In Situ Technique for the Study of Heterogeneous Catalysts. *Phys. Chem. Chem. Phys.* **2020**, *22*, 18747−18756.
(21) Ye, Y.; Wu, C. H.; Zhang, L.; Liu, Y.-S.; Glans-Suzuki, P.; Guo, J. Using Soft X-ray Absorption Spectroscopy to Characterize Electrode/Electrolyte Interfaces *In-Situ* and *Operando*. *J. Electron Spectrosc. Relat. Phenom.* **2017**, *221*, 2−9.
(22) Drake, I. J.; Liu, T. C. N.; Gilles, M.; Tyliszczak, T.; Kilcoyne, A. L. D.; Shuh, D. K.; Mathies, R. A.; Bell, A. T. An In Situ Cell for Characterization of Solids by Soft X-ray Absorption. *Rev. Sci. Instrum.* **2004**, *75*, 3242.
(23) Velasco-Velez, J.-J.; Wu, C. H.; Pascal, T. A.; Wan, L. F.; Guo, J.; Prendergast, D.; Salmeron, M. The Structure of Interfacial Water on Gold Electrodes Studied by X-Ray Absorption Spectroscopy. *Science* **2014**, *346*, 831−834.
(24) Wu, C. H.; Pascal, T. A.; Baskin, A.; Wang, H.; Fang, H.-T.; Liu, Y.-S.; Lu, Y.-S.; Guo, J.; Prendergast, D.; Salmeron, M. B. Molecular-Scale Structure of Electrode-Electrolyte Interfaces: The Case of Platinum in Aqueous Sulfuric Acid. *J. Am. Chem. Soc.* **2018**, *140*, 16237−16244.
(25) Van Spronsen, M.; Zhao, X.; Jaugstetter, M.; Escudero, C.; Duchoň, T.; Hunt, A.; Waluyo, I.; Yang, P.; Tschulik, K.; Salmeron, M. B. Interface Sensitivity in Electron/ion Yield X-ray Absorption Spectroscopy. The TiO_2−H_2O Interface. *J. Phys. Chem. Lett.* **2021**, *12*, 10212−10217.
(26) Jiang, P.; Prendergast, D.; Borondics, F.; Porsgaard, S.; Giovanetti, L.; Pach, E.; Newberg, J.; Bluhm, H.; Besenbacher, F.; Salmeron, M. B. Experimental and Theoretical Investigation of the Electronic Structure of Cu_2O and CuO Thin Films on Cu(110) Using X-ray Photoelectron and Absorption Spectroscopy. *J. Chem. Phys.* **2013**, *138*, 024704.
(27) Jiang, P.; Chen, J.-L.; Borondics, F.; Glans, P.-A.; West, M. W.; Chang, C.-L.; Salmeron, M. B.; Guo, J. In situ Soft X-ray Absorption Spectroscopy Investigation of Electrochemical Corrosion of Copper in Aqueous $NaHCO_3$ Solution. *Electrochem. Commun.* **2010**, *12*, 820−822.
(28) Chou, T.-C.; Chang, C.-C.; Yu, H.-L.; Yu, W.-Y.; Dong, C.-L.; Velasco-Vélez, J.-J.; Chuang, C.-H.; Chen, L.-C.; Lee, J.-F.; Chen, J.-M.; Wu, H.-L. Controlling the Oxidation State of the Cu Electrode and Reaction Intermediates for Electrochemical CO_2 Reduction to Ethylene. *J. Am. Chem. Soc.* **2020**, *142*, 2857−2867.
(29) Weatherup, R. S.; Wu, C. H.; Escudero, C.; Pérez-Dieste, V.; Salmeron, M. B. Environment-Dependent Radiation Damage in Atmospheric Pressure X-ray Spectroscopy. *J. Phys. Chem. B* **2018**, *122*, 737−744.
(30) Gann, E.; Young, A. T.; Collins, B. A.; Yan, H.; Nasiatka, J.; Padmore, H. A.; Ade, H.; Hexemer, A.; Wang, C. Soft X-ray Scattering Facility at the Advanced Light Source with Real-Time Data Processing and Analysis. *Rev. Sci. Instrum.* **2012**, *83*, 045110.
(31) McAfee, T.; Ferron, T.; Cordova, I. A.; Pickett, P. D.; McCormick, C. L.; Wang, C.; Collins, B. A. Label-free Characterization of Organic Nanocarriers Reveals Persistent Single Molecule Cores for Hydrocarbon Sequestration. *Nat. Commun.* **2021**, *12*, 3123.
(32) Zhong, W.; Liu, F.; Wang, C. Probing Morphology and Chemistry in Complex Soft Materials with In Situ Resonant Soft X-Ray Scattering. *J. Condens. Matter Phys.* **2021**, *33*, 313001.
(33) Holtz, M. E.; Yu, Y.; Gunceler, D.; Gao, J.; Sundararaman, R.; Schwarz, K. A.; Arias, T. A.; Abruña, H. D.; Muller, D. A. Nanoscale Imaging of Lithium Ion Distribution during In Situ Operation of Battery Electrode and Electrolyte. *Nano Lett.* **2014**, *14*, 1453−1459.
(34) Yang, Y.; Shao, Y.-T.; Lu, X.; Abruña, H. D.; Muller, D. A. Elucidating Cathodic Corrosion Mechanisms with *Operando* Electrochemical Liquid-Cell STEM in Multiple Dimensions. *Microsc. Microanal.* **2021**, *27*, 238−239.
(35) Yang, Y.; Shao, Y.-T.; DiSalvo, F. J.; Muller, D. A.; Abruna, H. D. Metal Monolayers on Command: Underpotential Deposition at Nanocrystal Surfaces: A Quantitative *Operando* Electrochemical Transmission Electron Microscopy Study. *ACS Energy Lett.* **2022**, *7*, 1292−1297.
(36) Yu, S.; Kim, D.; Qi, Z.; Louisia, S.; Li, Y.; Somorjai, G. A.; Yang, P. Nanoparticle Assembly Induced Ligand Interactions for Enhanced Electrocatalytic CO_2 Conversion. *J. Am. Chem. Soc.* **2021**, *143*, 19919−19927.
(37) Frahm, R. New Method for Time Dependent X-Ray Absorption Studies. *Rev. Sci. Instrum.* **1989**, *60*, 2515−2518.
(38) Joly, L.; Otero, E.; Choueikani, F.; Marteau, F.; Chapuis, L.; Ohresser, P. Fast Continuous Energy Scan with Dynamic Coupling of the Monochromator and Undulator at the DEIMOS Beamline. *J. Synchrotron Radiat.* **2014**, *21*, 502−506.

https://doi.org/10.1021/jacs.2c03662
J. Am. Chem. Soc. 2022, 144, 8927−8931